High-Efficiency DAB Converter Using Switching Sequences and Burst Mode

Germán G. Oggier, *Member, IEEE*, and Martin Ordonez, *Member, IEEE*

***Abstract*—Dual active bridge converters enable bidirectional power flow in buck and boost operating modes. This paper presents an advanced switching sequence and burst-mode strategy to balance conduction, switching, and magnetic losses under light, medium, and heavy loading conditions, leading to improved operating efficiency. The implementation of the switching sequence employs the natural state-plane trajectories of the converter and contributes to higher efficiency and the ability to perform burst mode. The proposed switching sequences improve the overall efficiency of the converter by enabling soft switching and adjusting the frequency to match the minimum RMS transformer current in the full operating range. Furthermore, it incorporates a fully controlled burst-mode switching sequence for light loading conditions to further extend the efficiency gains. As a result, maximum efficiency is obtained by taking advantage of all the possible switching structures of the converter. The analysis provides insight into the natural trajectories of the converter, which produce soft-switching transitions and enable the converter structures to achieve the target operating point directly. Simulation and experimental results are presented to validate the benefits of the switching sequence and illustrate the burst-mode operation.**

***Index Terms*—Boundary control, dc–dc isolated converters, dual active bridge (DAB) converter.**

I. Introduction

BIDIRECTIONAL power converters are a core requirement for many different power electronic conversion applications [1]–[3] (such as backup systems, regenerative motor drives, plug-in hybrid electric vehicles, microgrids, distributed generation systems, and renewable energy applications with intermediate energy storage) and are necessary in order to adapt different voltage levels and control the power flow between the different components [4], [5].

In this context, the dual active bridge (DAB) converter shown in Fig. 1(a) provides an effective means to implement power interfaces, since it enables bidirectional power flow control and can operate in both buck and boost modes, with fast transient response [6]–[8]. The DAB converter has also been investigated for high-power applications and is considered an essential component of modern smart grids and microgrids, as it enables bidirectional power flow between the source and the load [9]–[12].

By using a traditional modulation strategy, it is possible to achieve high efficiency in the DAB converter owing to soft switching, but only in a reduced operation region. This limitation is a function of the voltage conversion ratio and the output current [13]. In order to solve this problem, many efforts have been made to maximize overall efficiency. These mainly consist of ensuring operation under soft switching throughout an extended region by applying modified modulation strategies in order to force soft-switching transitions [14]–[20]. These strategies generally also improve the form factor of the current through the transformer, therefore reducing losses and mitigating harmonics. In this way, improvements in the overall performance can be achieved [15]. The strategy developed in [21] takes advantage of the discontinuous-current mode, which enables the reduction of diode reverse recovery losses, owing to the zero current switching transitions, and thereby benefits light loading operation. One of the key parameters in the operation of the DAB converter is the value of the transformer leakage inductance. The power transfer can be improved by controlling the series reactance and the reactive power [7], [14] between the two active bridges, which is proportional to the transformer leakage inductance. Recent proposals use a modulation strategy where the series reactance is adjusted by changing the switching frequency, as a function of the converter operation point, to ensure zero-voltage switching [22], [23]. The strategy of changing the switching frequency has been extensively used for resonant converters in the manner proposed in [24], where a three-level isolated *LLC* resonant converter using a novel modulation strategy for wide-voltage range operation is employed. This strategy allows the dc gain of the converter to be changed between width ratios by varying the switching frequency of the converter. As a result, the converter can be designed to operate within a narrow operation condition, maintaining high efficiency despite wide-voltage range variations.

The efficient operation of DAB converters is challenging and requires dealing with a wide range of operating conditions (from light to heavy loads) while minimizing losses in all the elements of the converter (passive and active) to mitigate conduction, switching, and magnetic power dissipation. For example, under light load conditions, the soft-switching mode is difficult to obtain, and therefore, switching losses become predominant (conduction and magnetic losses are low). On the other hand, losses in medium loading condition are balanced, while heavy loading condition produces high conduction losses (RMS current) in the switches and magnetic devices. Therefore, efficient and improved DAB operation must involve the accurate

Manuscript received February 2, 2015; revised April 14, 2015; accepted May 19, 2015. Date of publication June 3, 2015; date of current version November 16, 2015. Recommended for publication by Associate Editor C. N. M. Ho.

G. G. Oggier is with the Department of Electrical and Computer Engineering, University of British Columbia, Vancouver, BC V6T 1Z4 Canada, and also with the Consejo Nacional de Investigaciones Cientificas y Tecnicas, C1040AAH Buenos Aires, Argentina (e-mail: goggier@ieee.org).

M. Ordonez is with the Department of Electrical and Computer Engineering, University of British Columbia, Vancouver, BC V6T 1Z4 Canada (e-mail: mordonez@ieee.org).

Color versions of one or more of the figures in this paper are available online at http://ieeexplore.ieee.org.

Digital Object Identifier 10.1109/TPEL.2015.2440753

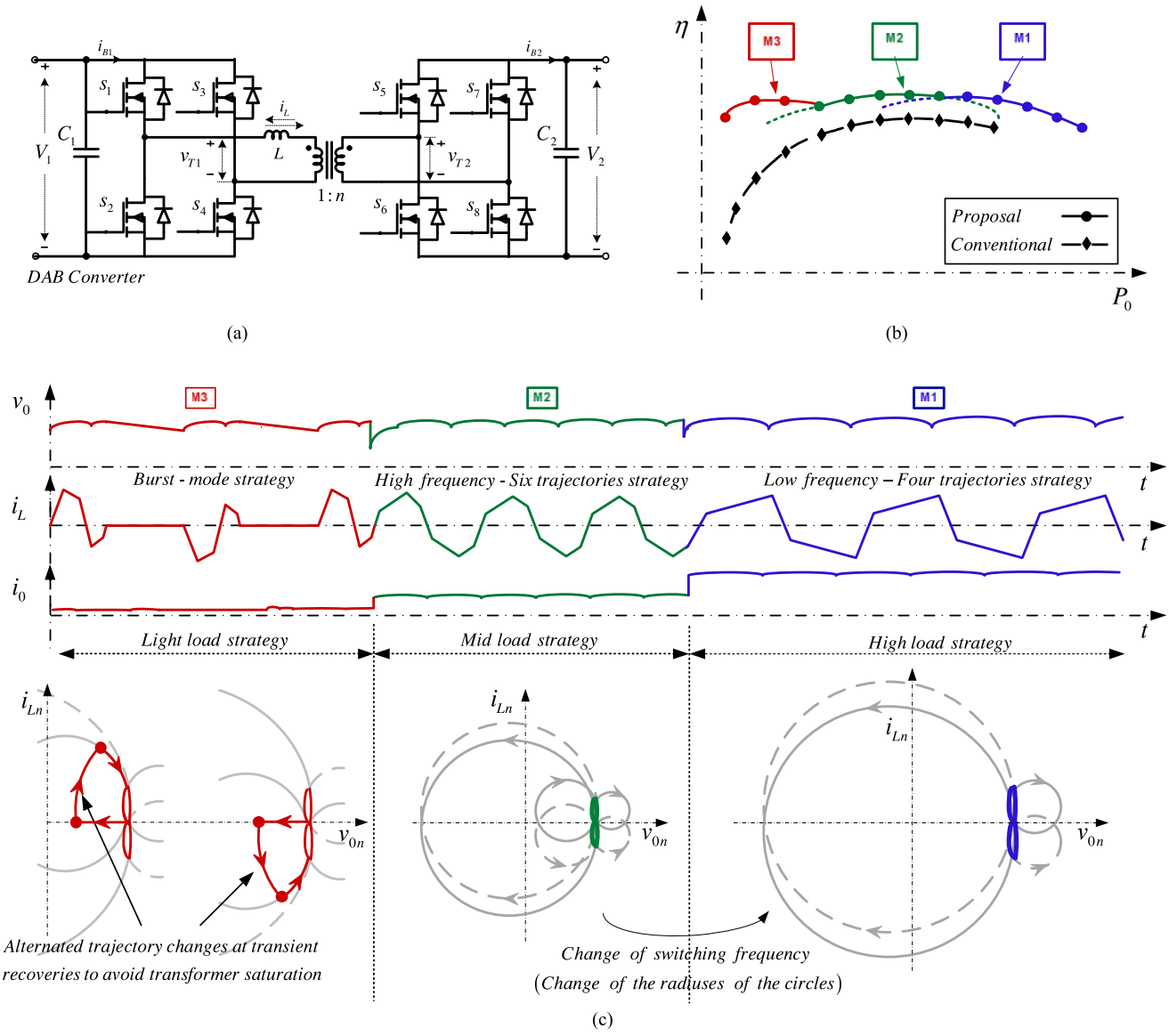

Fig. 1. (a) Simplified scheme of the DAB converter. (b) Comparison of efficiency by using the conventional and the proposed strategies. (c) Conceptual time-domain waveforms and phase-plane strategies to operate the converter under light, medium, and high load using the proposed strategies.

control of multiple mechanisms (such as frequency, soft transitions, RMS current, and power flow simultaneously).

This paper presents an advanced switching sequence and burst-mode strategy to balance conduction, switching [25] and [26], and magnetic losses under light, medium, and heavy loading conditions, leading to improved operating efficiency in the entire operating range. A new framework based on trajectory analysis is presented and results in accurate control of switching sequences, frequency, and RMS current, in order to obtain higher efficiency from light to 100% loading condition. The ability to control the trajectories of the converter provides a significant opportunity in the form of a burst-mode switching sequence for light loads. This technique consists of turning ON the converter for a few switching cycles when a small or light load is present, reducing unnecessary switching and conduction power losses in the switches and, thus, increasing operating efficiency.

The conceptual efficiency gains are presented in Fig. 1(b), depicting three operating regions each for heavy (region M1), medium (M2), and light (M3).

The proposed switching sequences are shown conceptually in Fig. 1(c), which depicts time-domain waveforms and phase planes, and in which different modes (M1, M2, and M3) are shown that have been chosen as function of the output power. When the load of the converter is close to the maximum output power, the control scheme selects a minimal switching sequence M1 (four trajectories) and applies an advantageous lower frequency operation which is selected to minimize the RMS current of the transformer. Under medium loading condition, the switching frequency is increased inversely with the output current, and

the modulation strategy M2 employs six natural trajectories in order to minimize the total converter losses. With the proposed six trajectory strategy (M2), soft-switching transition are obtained. An additional feature made possible by manipulating the natural state-plane trajectories is the burst-mode switching sequence (M3) for light loading conditions. Burst sequence M3 involves turning ON the converter for a few switching cycles to charge the output capacitor and support a light load with improved efficiency. The M3 burst sequence prevents unnecessary switching actions and conduction losses in the power switches.

The natural state-plane trajectories employed in this study provide significant insight into the operation of the converter and lead to enhanced switching sequences to cover the whole loading range of the converter. Simulation and experimental results using a DAB converter validate the theory and concepts proposed in this study.

II. DAB Topology and Normalized Derivation

The DAB topology consists of a full bridge working as a dc–ac converter, feeding a high-frequency transformer, which supplies a second full bridge working as an ac–dc converter. The analysis of the DAB converter could be simplified by referring the model to one side of the transformer and considering the transformer model to be represented only by its leakage inductance [13].

The conventional modulation strategy consists of controlling both bridges in order to generate a constant-frequency voltage waveform. The power flow is controlled by manipulating the phase shift between the voltages of the transformer terminals v_{T1} and v_{T2} [6]. The switching frequency to operate the converter using the conventional strategy is fixed at 10 kHz. The modified strategy uses special switching sequences under light, medium, and heavy loading conditions to improve the system efficiency in the whole operating range.

The derivation of the natural trajectories of the converter is presented to cover the different operating modes. Power flow from v_1 to v_2 is considered, called hereinafter as V_{cc} and v_0, respectively. The converter can be represented by a system of differential equations as follows:

$$\frac{dv_0}{dt} = \frac{1}{C}\left(i_L u_2 - i_0\right) \tag{1}$$

$$\frac{di_L}{dt} = \frac{1}{L}\left(V_{cc}u_1 - v_0 u_2\right). \tag{2}$$

The voltage applied to leakage inductance (L) can take different active levels depending on the state of the switches. According to the waveforms represented in Fig. 2, when the converter operates with the switching sequence corresponding to M1, there are four different structures, while for the switching sequence corresponding to M2, there are six structures. For this particular case, the voltage applied to the leakage inductance takes the following values:

$$\text{For buck mode}: \ (V_{cc}+v_0),\ (V_{cc}-v_0),\ (-v_0)$$
$$(-V_{cc}-v_0),\ (-V_{cc}+v_0),\ \text{and}\ (v_0).$$

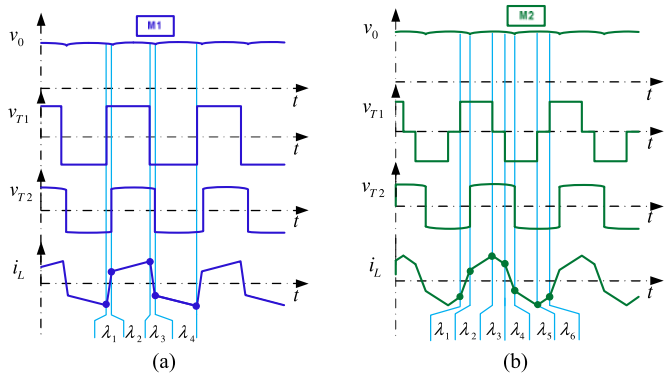

Fig. 2. Main waveforms of the DAB converter for buck mode: (a) M1 and (b) M2.

$$\text{For boost mode}: \ (V_{cc}+v_0),\ (V_{cc}),\ (V_{cc}-v_0)$$
$$(-V_{cc}-v_0),\ (-V_{cc}),\ \text{and}\ (-V_{cc}+v_0).$$

These cases are represented in (1) and (2) by $u_1 = 1$ for $v_{T1} = V_{cc}$, $u_1 = 0$ for $v_{T1} = 0$, and $u_1 = -1$ for $v_{T1} = -V_{cc}$. In addition, for the second bridge, B_2, the different cases are represented by $u_2 = 1$ for v_0 and $u_2 = -1$ for $-v_0$. When the converter operates in boost mode, the zero state is only possible in bridge B_2 [15].

In order to simplify the mathematical representation of the converter, a normalization technique is employed to disengage some of the parameters of the converter. The normalization is performed by using the characteristic impedance of the combined L and C values, $Z_0 = \sqrt{L/C}$, natural frequency $f_0 = 1/T_0 = 1/\left(2\pi\sqrt{LC}\right)$, and the converter reference voltage, V_r, as base quantities, as follows:

$$v_{xn} = \frac{v_x}{V_r} \tag{3}$$

$$i_{xn} = \frac{i_x}{V_r} Z_0 \tag{4}$$

$$t_n = t.f_0 \tag{5}$$

where v_x and i_x represent generic voltages and currents, and v_{xn} and i_{xn} their respective normalized values.

After performing normalization, (1) and (2) can be rewritten as

$$\frac{dv_{0n}}{dt_n} = 2\pi\left(i_{Ln}u_2 - i_{0n}\right) \tag{6}$$

$$\frac{di_{Ln}}{dt_n} = 2\pi\left(V_{CCn}u_1 - v_{0n}u_2\right). \tag{7}$$

By combining (6) and (7), a general second-order differential equation is obtained

$$\frac{d^2 i_{Ln}}{dt_n^2} = 4\pi^2 u_2\left(i_{0n} - i_{Ln}u_2\right). \tag{8}$$

The solution of this second-order system can be written as

$$i_{Ln} = A\cos\left(\beta t_n\right) + B\sin\left(\beta t_n\right) + i_{0n}u_2 \tag{9}$$

where $A = \left(i_{Ln}(0) - i_{0n}u_2\right)$, $B = \left(di_{Ln}(0)/dt_n\right)/\beta$, and $\beta = 2\pi$.

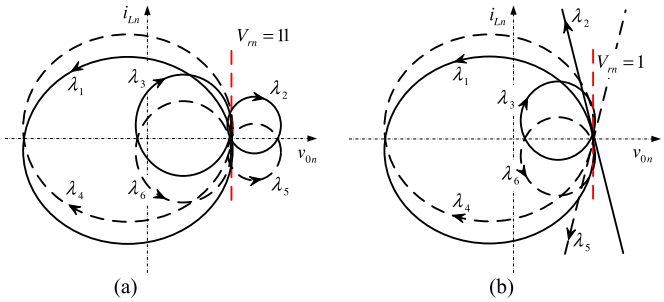

Fig. 3. Normalized natural trajectories for the DAB converter. (a) Buck mode. (b) Boost mode.

At the target operating point $i_{Ln}(0) = i_{Ln,\text{target}}$ u_2 is derived in order to operate the converter at a desired switching frequency and $v_{on} = V_{rn}$, where

$$V_{rn} = 1. \tag{10}$$

By using trigonometric identities and performing a transformation process, the normalized time, t_n, can be eliminated from (1) and (2) after using (3), (4), and (5), yielding the following expressions for the natural trajectories of the DAB converter for buck mode:

$$\lambda_{\{1-6\}} = (V_{ccn}u_1 - v_{0n}u_2)^2 - (i_{Ln\_\lambda x} - i_{0n}u_2)^2 - \\ -(V_{ccn}u_1 - u_2)^2 + (i_{Ln} - i_{0n}u_2)^2. \tag{11}$$

And for boost mode:

$$\lambda_{\{1,3,4,6\}} = (V_{ccn}u_1 - v_{0n}u_2)^2 - (i_{Ln\_\lambda x} - i_{0n}u_2)^2 - \\ (V_{ccn}u_1 - u_2)^2 + (i_{Ln} - i_{0n}u_2)^2 \tag{12}$$

$$\lambda_{\{2,5\}} = i_{Ln} + \frac{V_{ccn}u_1}{i_{0n}}v_{0n} - i_{Ln\_\lambda y} - \frac{V_{ccn}u_1}{i_{0n}}. \tag{13}$$

From these expressions, it can be deduced that the natural trajectories of the DAB converter for the different modes are circles and straight lines on the plane that shows the normalized inductor current versus the normalized output voltage of the converter using the proposed strategy. Fig. 3 shows the planes of the normalized inductor current versus the normalized output voltage, for buck and boost operating modes. Natural trajectories can be used for fast transient response [8], but the objective of this study is to do special modulations for high efficiency by using novel modes M1, M2, and M3.

In this paper, $i_{Ln,\text{target}}$ is derived in order to operate the converter with the desired switching frequency, which is selected as function of the required output power [see Fig. 1(c)]. Since the inductor current at the switching angles is a function of the switching frequency, terms of $i_{Ln\_\lambda x}$ and $i_{Ln\_\lambda y}$ given in previous expressions can be obtained from the steady-state inductor current expressions as follows [27]:

Solutions for buck mode

$$i_{L\_\lambda 1} = \frac{V_{cc}(d\pi - 2d\delta - m\pi)}{2\omega L} \tag{14}$$

$$i_{L\_\lambda 2} = \frac{V_{cc}(2\delta - m\pi + d\pi)}{2\omega L} \tag{15}$$

$$i_{L\_\lambda 3} = \frac{V_{cc}(2\delta d + m\pi + d\pi - 2dm\pi)}{2\omega L}. \tag{16}$$

Solutions for boost mode

$$i_{L\_\lambda 1} = \frac{V_{cc}(md\pi - \pi - 2d\delta)}{2\omega L} \tag{17}$$

$$i_{L\_\lambda 2} = \frac{V_{cc}(md\pi - \pi + 2\delta)}{2\omega L} \tag{18}$$

$$i_{L\_\lambda 3} = \frac{V_{cc}(\pi + md\pi - 2m\pi + 2\delta)}{2\omega L} \tag{19}$$

where δ is the phase shift between transformer primary voltage and secondary voltage, which can be determined as function of the required output power, $\omega = 2\pi f_s^*$ and f_s^* is the desired switching frequency, d is the voltage conversion ratio, and m is the modulation index, which are defined as

$$d = \frac{v_0}{(nV_{cc})} \tag{20}$$

and

$$m = \frac{\tau}{\pi} \tag{21}$$

respectively. In these expressions, n is the transformer turns ratio and τ is the width of the pulse generated by the bridge fed with the largest dc voltage. The modulation index could be determined in order to operate the DAB converter under soft-switching mode in the full operating range, as it is proposed in [15].

A. Range of Variation of the Switching Frequency

The switching frequency is selected as a function of the output power and it is modified between a minimum and a maximum value, as it is shown conceptually in Fig. 1(c). The maximum switching frequency at which the converter can be operated is limited by the semiconductor switching losses, as it is conceptually explained in Fig. 4(a), whereas the minimum switching frequency is determined by the maximum magnetizing current of the transformer, which does not produce core saturation, as is explained below.

The following basic transformer equations [28] provide insight into the effects of moderate changes in the switching frequency. Its capability is given by

$$S = \frac{(V_{B1\text{rms}}I_{B1\text{rms}} + V_{B2\text{rms}}I_{B2\text{rms}})}{2}. \tag{22}$$

The induced emf in a winding is determined according to Faraday's law of induction, which is proportional to the rate of change of the magnetic flux. The induced emf can also be expressed as function of the switching frequency as follows:

$$E = K_1 f_s B. \tag{23}$$

As discussed in [29], silicon steel sheet is normally used in large power converters for transmission or distribution power systems. By contrast, ferrite is often used in higher frequency operation for low- and medium-power converters. Amorphous and nanocrystalline materials are also popular to apply as core materials in medium-frequency transformers.

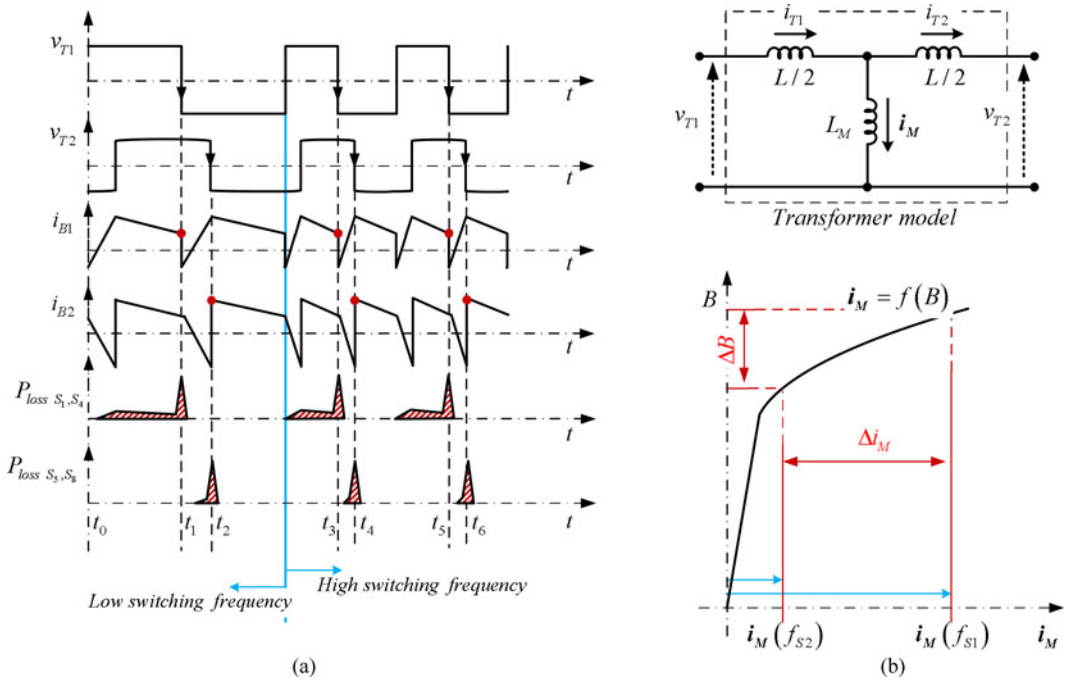

Fig. 4. (a) Conceptual switch power losses for two different switching frequencies: waveforms of i_{B1} and i_{B2} corresponds to the dc current of bridge B_1 and B_2, respectively. (b) Transformer model considering the magnetizing inductance (top) and variation of the magnetizing current as function of the induction of the core (bottom).

The total core losses comprise mainly the eddy current losses and the hysteresis losses, and in order to simplify the calculation of these losses, the transformer can be considered to be fed by a sinusoidal voltage waveform, and the following equation can be used: $P_{\rm core} = P_{ed} + P_{hy} = K_{c1} f_s^2 \hat{B}^x + K_{c2} f_s^y \hat{B}^z$, where K_{c1} and K_{c2} are constants given for the material of the core, and x, y, and z are exponent lying between 1 and 3 that can be established from the core datasheet. The winding resistive losses are functions of the RMS current $P_w = K_3 I_{\rm rms}^2$, and K_3 is a constant given for the resistance of the windings.

The magnetizing current is related to the core induction, which is function of the *B–H* loop of the magnetic core

$$i_M = f(B) \tag{24}$$

in which the magnetizing current increases faster than the core induction, B.

Thus, for a particular transformer, the capability of which is given by (22) and the amplitude of V_1 and V_2 are determined by the application, a change in the switching frequency produces an inversely proportional change in the core induction, B [see (23)]. On the other hand, the core losses will increase as switching frequency increases and the core induction will decrease in a squared ratio. As a consequence, the total transformer losses will be reduced when the switching frequency increases within moderate limits.

On the other hand, when the switching frequency increases, the magnetizing current is reduced by a greater proportion than the induction of the magnetic core, which is reduced according to the magnetization curve of the material, as it is shown in Fig. 4(b).

In conclusion, if the transformer is operated with a moderated higher frequency, the total losses will be lower, as will be the magnetizing current. In this manner, a moderate increase in frequency establishes a mechanism can be used to improve the efficiency of the converter under certain loading conditions.

III. Efficiency Improvement Strategy

In this section, the proposed strategy to operate the DAB converter efficiently is presented, covering the entire loading range. As mentioned in previous sections, in order to operate the converter with maximum efficiency for all values of the output power, different switching sequences are used. In this paper, the switching frequency is adjusted to minimize the RMS transformer current as a function of the output power, which allows the conduction and transformer winding losses to be minimized. Since MOSFET power switches are employed in the converter operating at moderate frequencies, conduction losses play a dominant role as part of the total efficiency of the system.

The RMS transformer current is defined in steady state as follows:

$$I_{L\ \rm rms} = \sqrt{\frac{1}{\pi}\int_0^{\pi} (i_L(\theta))^2 d\theta} \tag{25}$$

where $i_L(\theta)$ can be established for the different structures shown in Fig. 2(a) and (b).

By solving (25), the expressions given in Table I can be obtained, valid for buck and boost operating modes.

TABLE I
TRANSFORMER RMS CURRENT

Buck mode and $\delta > 0°$	$\frac{1}{6}\sqrt{3}V_1 \frac{\sqrt{\left(d^2\pi^4 + 2\frac{m^2\pi^3\sqrt{a}}{V_1} - 4\frac{\sqrt{a}P_0\omega L\pi^2}{dV_1{}^3} - 4\frac{\sqrt{a}m\pi^3}{V_1} + 3m^2\pi^2 - 2m^3\pi^4\right)}}{\omega L\pi}$
Buck mode and $\delta < 0°$	$\frac{1}{6}\sqrt{3}V_1 \frac{\sqrt{\left(d^2\pi^2 + m^3\pi^2 d - 3dm\pi^2 + 12\frac{(P_0\omega L)^2}{dmV_1{}^4} + 3m^2\pi^2 - 2m^3\pi^2\right)}}{\omega L}$
Boost mode and $\delta > 0°$	$\sqrt{\frac{-\frac{1}{12}\left(-3d^4V_1{}^3m^2\pi^3 + 2d^4V_1{}^3m^3\pi^3 - 3\sqrt{b}(dV_1m\pi)^2 - \sqrt{b^3} + 6\sqrt{b}m(dV_1\pi)^2 - \pi^3d^2V_1{}^3\right)}{V_1\pi(d\omega L)^2}}$
Boost mode and $\delta < 0°$	$\frac{1}{6}V_1 \frac{\sqrt{\left(-6m^3d^2\pi^2 + 9m^2\pi^2d^2 + 3dm^3\pi^2 - 9m\pi^2d + 36\frac{(P_0\omega L)^2}{dmV_1{}^4} + 3\pi^2\right)}}{\omega L}$

where $a = 2m(V_1 d\pi)^2 - (dV_1 m\pi)^2 - 4dP_0\omega L\pi$ and $b = -d\pi\left(V_1{}^2 dm^2\pi + 4P_0\omega L - 2V_1{}^2 dm\pi\right)$.

The efficiency is defined as function of the total DAB converter losses as follows:

$$P_T = I_{S\,\mathrm{rms}}^2 R_{d\mathrm{son}} + \frac{1}{2} I_p V_x t_c f_{\mathrm{sw}} + I_{L\,\mathrm{rms}}^2 R_{cu} + P_{\mathrm{core}}. \quad (26)$$

The two first terms correspond to switch conduction and switching losses, respectively; the third term corresponds to transformer winding losses. In relation to skin effect and associated losses, the effect of increase the winding resistances of the transformer can be estimated from the datasheet of the manufacturer. $I_{S\,\mathrm{rms}}$ is the RMS current of the power switches and is proportional to the RMS transformer current; $R_{d\mathrm{son}}$ is the equivalent MOSFET on-resistance; I_p is the summation of the transformer current at the switching angles; V_x is the dc voltage of the bridge x, and the t_c is the time of the turn-on/off transition of the power switches. The P_{core} represents the losses associated with the magnetic core, which depend on the magnetic flux, the frequency, the core volume, and the voltage waveform, which can be modeled as proposed in [30] . Thus, the efficiency can be expressed as $\eta = P_0/(P_0 + P_T)$, where P_0 is the output power.

Fig. 5 shows the evolution of the DAB converter's efficiency versus the output power, according to (26), when the switching frequency is modified between 6 and 10 kHz using the different switching sequences. The implementation is made with MOSFETs for a 1-kW prototype, an input voltage of 50 V, and an output voltage of 100 V. M1, M2, and M3 strategies are depicted, along with the efficiency obtained through the conventional modulation strategy, using the parameters of the implemented DAB converter. It can be observed that for each output power, there is a maximum efficiency that can be obtained for each switching frequency and switching sequence.

These results clearly suggest that the different switching sequences and the switching frequencies have a significant impact on the efficiency of the converter. What follows is a detailed description of the switching strategies M1, M2, and M3.

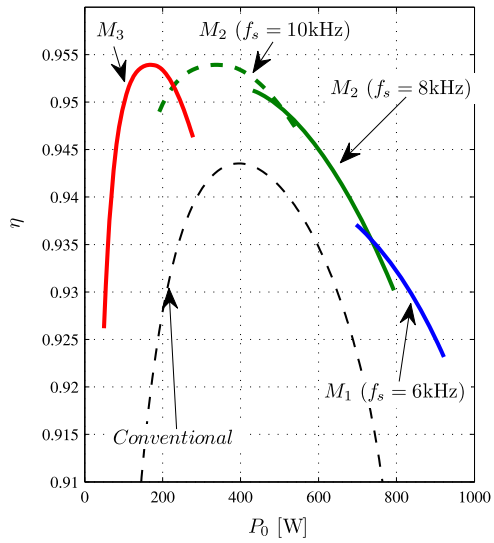

Fig. 5. Theoretical efficiency versus output power with the switching sequence and frequency as a parameter.

A. Four Trajectories Strategy—M1

This strategy is selected for high output loading condition, which is characterized by switching between four natural trajectories by satisfying the next sequence in a full switching period: $\lambda_1 \rightarrow \lambda_2 \rightarrow \lambda_4 \rightarrow \lambda_5$ for buck mode and $\lambda_1 \rightarrow \lambda_3 \rightarrow \lambda_4 \rightarrow \lambda_6$ for boost mode, where the different trajectories are defined in Section II for each mode.

This strategy improves the efficiency of the DAB converter when the output power is high because the soft-switching operating mode is ensured. Furthermore, for the same value of switching frequency, the ability to operate the converter using the switching strategy M1 allows more power to be transferred than any other sequence under soft-switching mode. This is because the structures λ_3 and λ_6 [shown in Fig. 2(b)] have the effect of reducing the maximum power that can be transferred and should be avoided with heavy loading condition. Sequences

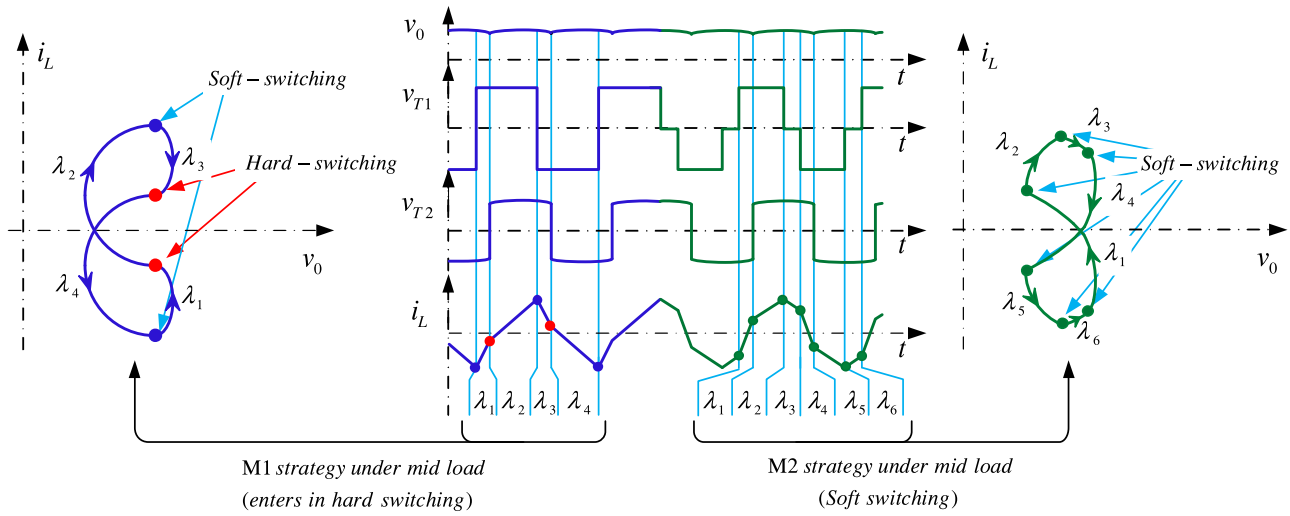

Fig. 6. Phase-plane and time-domain waveforms using the strategy M1 (left) and the strategy M2 (right). M1 works very well for high loading condition but enters in hard switching under mid loading.

with six trajectories (such as M2) are not recommended under heavy loads due to the power transfer capability reduction limited by high series reactance. M1 enhances power transfer with soft transitions and also allows a moderate switching frequency reduction to utilize the transformer magnetization capacity, and consequently, the losses due to the RMS current are restricted proportionally to the reduction of the switching frequency.

B. Six Trajectories Strategy—M2

When the output power decreases, the converter can start operating under hard-switching mode if the strategy M1 is used. Consequently, the total converter losses can increase considerably. Soft-switching constraints dictate that the current at the interval corresponding to λ_2 for M1 and intervals corresponding to λ_2 and λ_3 for M2, defined in Fig. 2, must be positive [13]. Switching sequence M1 can operate under soft switching within a reduced range of operation, depending on the voltage conversion ratio and on the output current, which is limited to a high-power range. When the output power decreases, the converter can start operating in hard switching mode, making it necessary to change the switching strategy in order to modify the transformer current waveform. To maximize the efficiency of the DAB converter for the medium power range, the controller selects the strategy M2, which allows the current waveform to be modified properly by using six different structures, defined in Section II. This situation is shown conceptually in Fig. 6: the DAB converter operates under hard-switching mode when M1 is used (left phase plane), and under soft switching when strategy M2 is used (right phase plane). As a result, soft-switching transitions are ensured by enabling new combinations in the structures of the converter.

In order to maintain the balance of the transformer current, the next sequence has to be satisfied in a full switching period for mid load range: $\lambda_1 \rightarrow \lambda_2 \rightarrow \lambda_3 \rightarrow \lambda_4 \rightarrow \lambda_5 \rightarrow \lambda_6$, where the general expressions of λ are given in (11)–(13).

When a change in the output voltage reference or load occurs, the natural trajectories given in (6) change their respective centers and radiuses to match the new operating condition, and the operating point will be located outside of the figure delimited by the steady-state natural trajectories. Then, the control strategy selects the sequence in order to reach the boundary of the plane that determines steady-state operation with minimum switching actions. Thereafter, a change in the structure of the system is performed (u_1 and/or u_2 changes) to force the operating point to follow the perimeter of the plane.

Fig. 7 shows the evolution of the normalized output voltage and normalized inductor current for different initial conditions marked as A and B, for both operating modes. For example, by analyzing the initial condition A in Fig. 7(a), two possible solutions can be employed to reach the target. The first option consists of turning ON S_1, S_4, S_5, and S_8 power switches in order to allow variables to evolve according to natural trajectory λ_2 (straight lines) while $\lambda_4 < 0$. Once λ_4 becomes positive, then turn ON S_2, S_3, S_5, and S_8 power switches to obtain a structure corresponding to natural trajectory λ_4. The second option consists of changing the natural trajectory λ_2 by λ_4 until λ_3 becomes positive. The difference between each options is made clear by analyzing Fig. 7(a), where a lower peak current is achieved using the first option and a higher peak current is obtained using the second option. It is interesting to note in Fig. 7 that a proper trajectory selection improves the behavior of the converter in transient mode. Moreover, the six-trajectory strategy of M2 provides increased efficiency in steady-state operation, as will be demonstrated through experimental results.

A similar analysis can be made of the different initial points (A and B) in the buck and boost operating modes shown in Fig. 7. It should be noted that the initial condition A [boost mode in Fig. 7(b)] provides two options to resolve the transient: λ_1 and λ_2. The λ_2 provides better dynamic voltage regulation (less voltage drop) than λ_1 and results in the same maximum

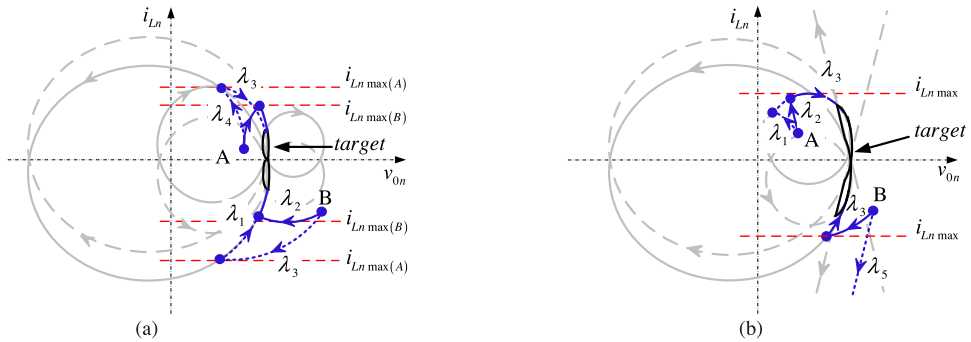

Fig. 7. Switching trajectories for the DAB converter using switching sequence M2. (a) Buck mode. (b) Boost mode.

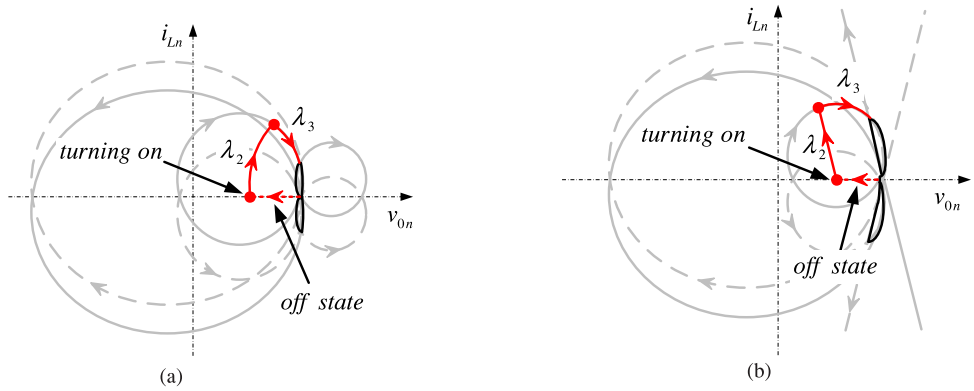

Fig. 8. Burst-mode switching sequence strategy for the DAB converter. (a) Buck mode. (b) Boost mode.

current when arriving at λ_3. For the initial condition marked as B in Fig. 7(b), only one option is possible (λ_3).

C. Burst-Mode Switching Sequence—M3

The ability to control the trajectories of the converter opens a significant opportunity in the form of a burst-mode switching sequence for light loading condition. This technique consists of turning on the converter for a few switching cycles when a small or light load is present, reducing unnecessary switching and conduction power losses in the switches, and thus increasing the efficiency of the converter.

Fig. 8 shows the burst-mode switching strategy for the DAB converter for both operating modes: buck and boost. Once the converter is turned OFF, the converter output voltage is reduced, due to the presence of the converter load, to a predefined minimum value, for instance 5% or 10% according to the requirements of the load. At this point, the converter is turned ON again and the control strategy selects the proper trajectories to reach the target, as is shown in Fig. 8 for buck and boost operating modes.

The mechanism to prevent saturation is achieved by means of reversing the trajectories selected to increase the output voltage. The case shown in Fig. 8 corresponds to half period using trajectories λ_2 while the operating point reaches λ_3, and then, the natural trajectory λ_3 is chosen. For the next half period, the natural trajectories selected to keep a volt–second balance are λ_5 while the operating point reaches λ_6, and then switch to λ_6.

This useful new feature in the form of burst mode results from the manipulation of the natural trajectories of the converter and results in a significant improvement in efficiency under light loading condition. Simulation and experimental evidence will be discussed in the following sections.

TABLE II
EXPERIMENTAL PROTOTYPE CHARACTERISTICS

Maximum output power ($P_{0\,\max}$)	1000 W
Switching frequency (f_s)	6–10 kHz
Maximum output current ($I_{0\,\max}$)	25 A
Output voltage (V_0)	30–100 V
Input voltage (V_{cc})	30–50 V
Transformer turns ratio (n)	1
Total inductance (L)	40 μH
Output capacitor (C)	20 μF

IV. RESULTS

Simulations and experimental results of a DAB converter are presented in this section in both buck and boost modes to verify the theoretical analysis presented in previous Sections. Table II presents the converter specifications for a 1-kW prototype. Fig. 9 shows a block diagram of the experimental setup.

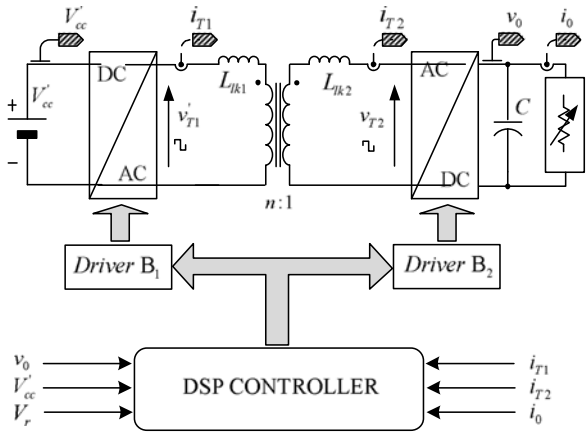

Fig. 9. Block diagram of the experimental setup.

The proposed efficient switching sequences were implemented using a TMS320F28035 fixed-point DSP. The processing power of the DSP defines how quickly the algorithm can be computed and, therefore, the maximum switching frequency of the converter. With the ongoing price reductions for high-performance DSP processors, the controller can be implemented at a reasonable cost. Hall-effect sensors are used in the implementation to measure current waveforms and voltage signals. It should be noted that the sensors selected to implement this advanced control technique are also used to protect the converter (typical input/output overcurrent and input/output overvoltage protections).

Fig. 10 shows the sequence of actions in the analog-to-digital converter interrupting routine considering the first half cycle for buck mode, which is called every time that the conversion of all the measured variables is completed.

Fig. 11 shows simulation results using the proposed strategy when the converter operates in boost mode with d =1.5 for three different output loads: the initial value of load current is i_o = 1 A and the controller selects the M3 mode; the output current then changes to i_o =6.5 A, and the controller selects the M2 mode with a switching frequency of 10 kHz; finally, the output current changes to i_o =13.5 A, and the controller selects the M1 mode with a switching frequency of 8 kHz. Fig. 12(a) shows the normalized state-plane trajectories during start-up and the transition from M3 to M2, and Fig. 12(b) shows the normalized state plane trajectories for the transition from M2 to M1.

It can observed that there is a smooth transition between the different switching sequences, due to the transformer current does not present a high value in order to reach the output voltage target when a change of load occurs. It can be observed in both Figs. 11 and 12 that the transformer current remains bounded when the output current changes from 1 to 6.5 A at 2 ms and then from 6.5 to 13.5 A at 3 ms.

As can be observed from these results, the operation of the converter is stable for the different loads and switching sequences, and during the transients when a change of load occurs. A constant output current loading condition is employed since

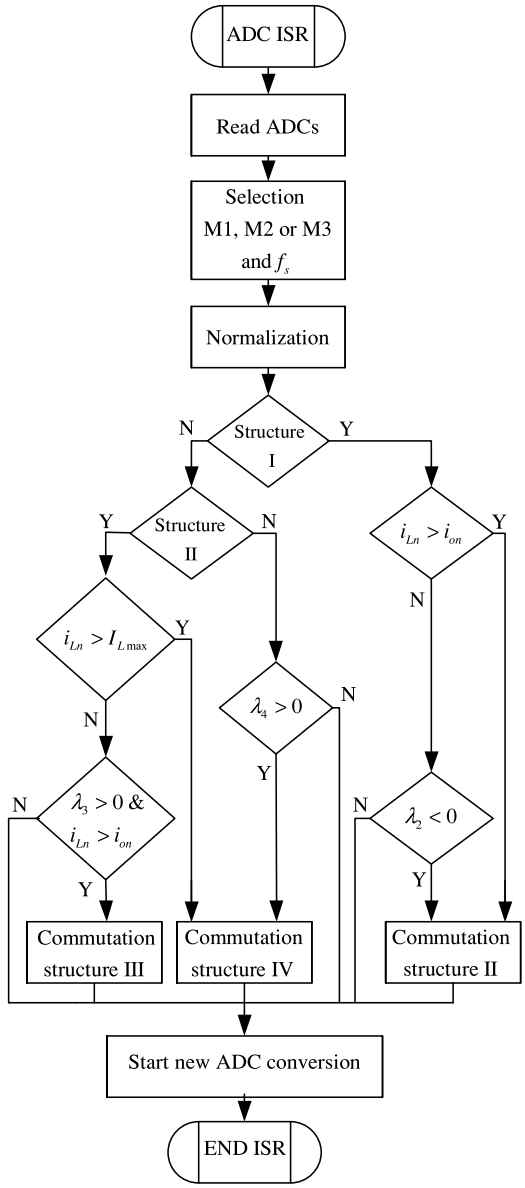

Fig. 10. DSP control algorithm flowchart for buck mode and M2 switching sequence.

it represents the worst-case scenario in terms of stability for positive equivalent resistance load: a situation where the system does not provide damping.

Fig. 13 shows start-up and steady-state experimental results. Fig. 13(a) corresponds to operation in buck mode when M1 switching sequence is used, while Fig. 13(b) shows the phase plane of the inductor current versus the output voltage for the same experiment. As predicted by the theory, the switching sequence is able to handle both start-up and steady-state operation, while following the natural trajectories explained in Section II. Experimental results for the switching sequence M2 are shown in Fig. 13(c) and (d) for buck mode and in Fig. 13(e) and (f) for boost mode, showing time-domain behavior along with the phase planes. During these transients, the strategy determines

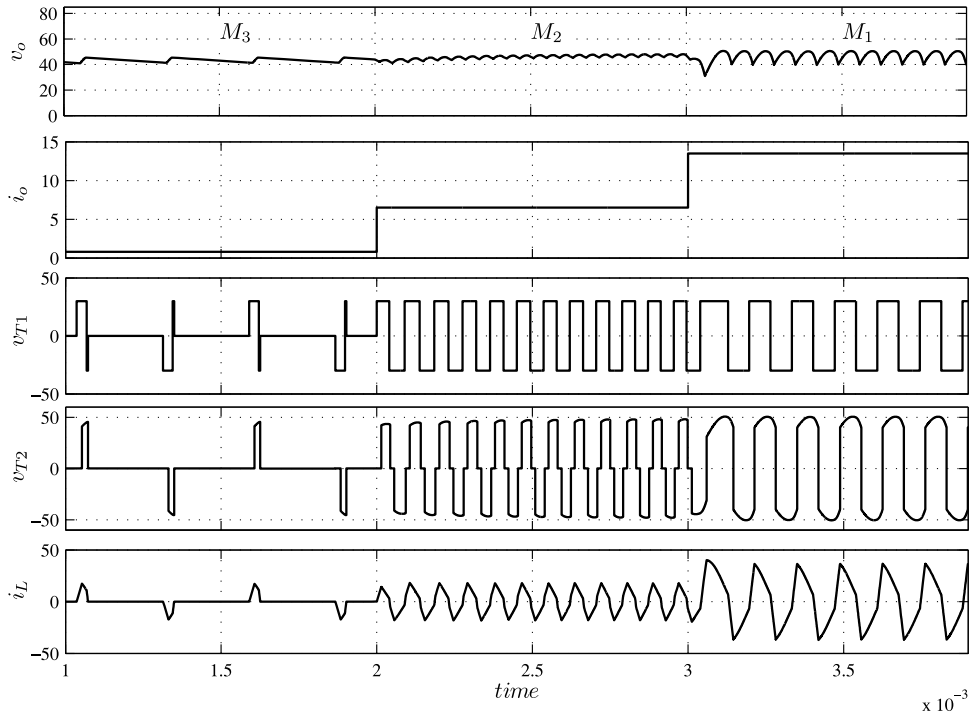

Fig. 11. Simulation results of the DAB converter using the proposed efficiency control strategy for three different output loads. When $i_o = 1$A, the M3 mode (burst) is selected; when i_o =6.5 A, the M2 mode is selected, and when i_o =13.5A, the M1 mode is selected.

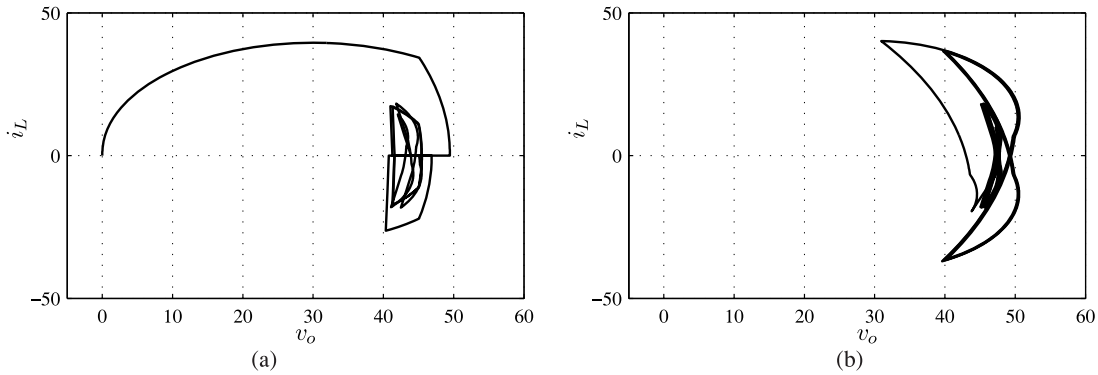

Fig. 12. Phase-plane simulation results of the DAB converter using the proposed efficiency control strategy for three different output loads. (a) Start-up and transition from M3 to M2. (b) Transition from M2 to M1.

the sequence explained in Section III-B, from time zero until steady state is reached. Hence, the response has no overshoot and steady state is reached in a few switching actions. For these results, the maximum inductor current is limited to 42 A in order to protect the switches of overcurrents during the start-up.

When the load of the converter is light, the strategy selects the burst-mode switching sequence (M3) in order to obtain a high efficiency. Fig. 14 shows the start-up and steady-state operation using this mode for two values of output power. Fig. 14(a) corresponds to $P_0 = 50$ W and Fig. 14(b) corresponds to $P_0 = 100$ W. During these transients, the volt–second magnetizing balance is controlled by alternating the polarity of the switching sequences to avoid saturation, as explained in Section III-C. It is interesting to note that the converter is operative for a fraction of the time (burst-mode operation), leading to higher efficiency. This advantageous operating mode, M3, is possible due to the ability of the strategy to manipulate the natural state-plane trajectories described in the theory.

Experimental results regarding changes to output voltage reference for buck mode are presented to validate the analysis presented in Section III-B regarding the selection of switching trajectories. Fig. 15(a) shows the response of the converter when the reference changes from 35 to 50 V in buck mode using M1 switching sequence. The converter reverts to steady state in only one switching action. The experimental results shown in Fig. 15(b)–(d) correspond to the converter operating in buck mode under M2 switching sequence for a reference changes from 25 to 35 V. Note that different transient resolution options (switching sequences) are used to reach the target operating point. As discussed in the theory presented in Section III, M2

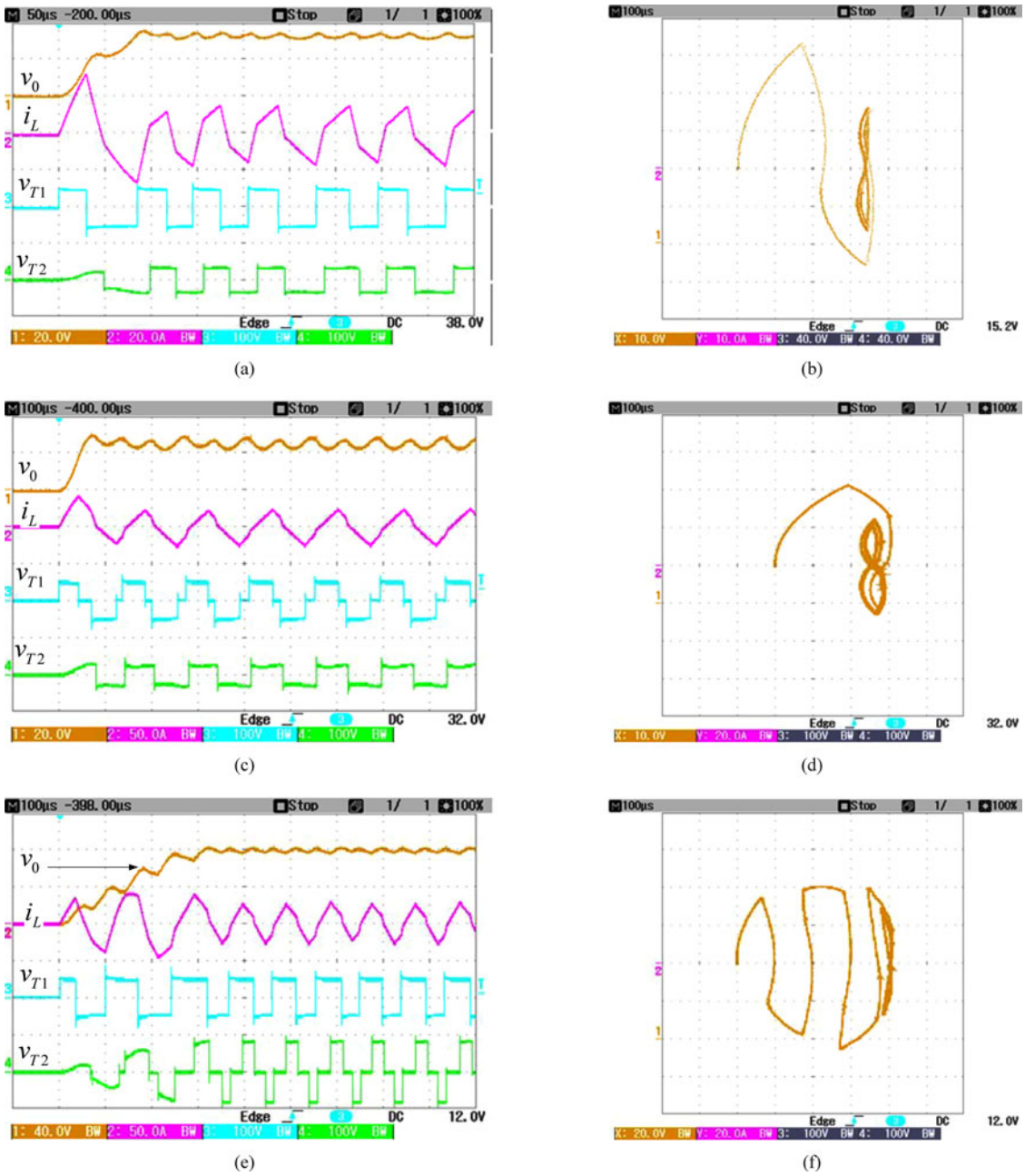

Fig. 13. Start-up and steady-state experimental results of the DAB converter using the strategy M1 for buck mode with $V_{cc} = 50$ V and $v_o = 35$ V for (a) time domain and (b) phase plane. Operation using the M_2 switching strategy in buck mode with $V_{cc} = 50$ V and $v_o = 27.5$ V for (c) time domain and (d) phase plane. Operation in boost mode with $V_{cc} = 50$ V and $v_o = 78$ V for (e) time domain and (f) phase plane. Output voltage (Ch1), inductor current (Ch2), primary voltage (Ch3), and secondary voltage (Ch4).

can resolve the transient with the sequence in Fig. 15(d) to avoid output voltage drop while keeping the current level low—this is the best transient resolution strategy. Fig. 15(b) shows the transient response obtained by choosing the natural trajectories λ_1, while the operating point reaches λ_3, after which λ_3 becomes the natural trajectory. Using this option, the output voltage drops (undesired) and inductor current peak is too high to reach steady-state operation. Fig. 15(c) shows the transient response obtained by choosing the natural trajectories λ_2 defined for boost mode while the operating point reaches λ_3 and, then, when the operating point reaches λ_3, choosing natural trajectories to follow. Using this trajectory, the inductor current peak is high (undesired) and the output voltage drop is minimal to reach steady state. Finally, Fig. 15(d) shows the transient response obtained by choosing the natural trajectories λ_2 corresponding to buck mode while the operating point reaches λ_3, and then, the transient response obtained when λ_3 becomes the natural trajectory used to reach steady-state operation. By using this switching sequence, the inductor current remains moderate and the output voltage is recovered without dropping. From the experimental results in

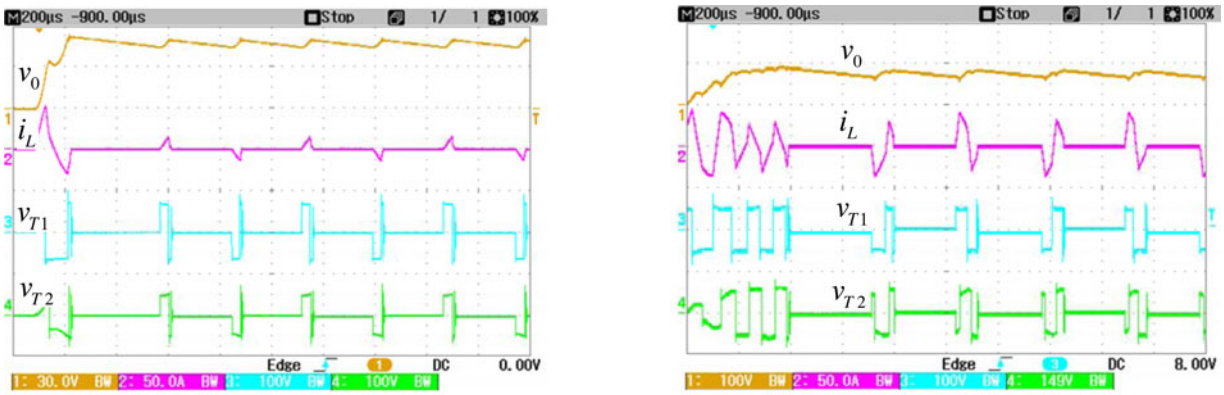

Fig. 14. Start-up and steady-state experimental results of the DAB converter using M3 burst-mode switching sequence with $V_{cc} = 30$ V and $v_o = 50$ V for (a) $P_0 = 50$ W and (b) $P_0 = 100$ W. Output voltage (Ch1), inductor current (Ch2), primary voltage (Ch3), and secondary voltage (Ch4).

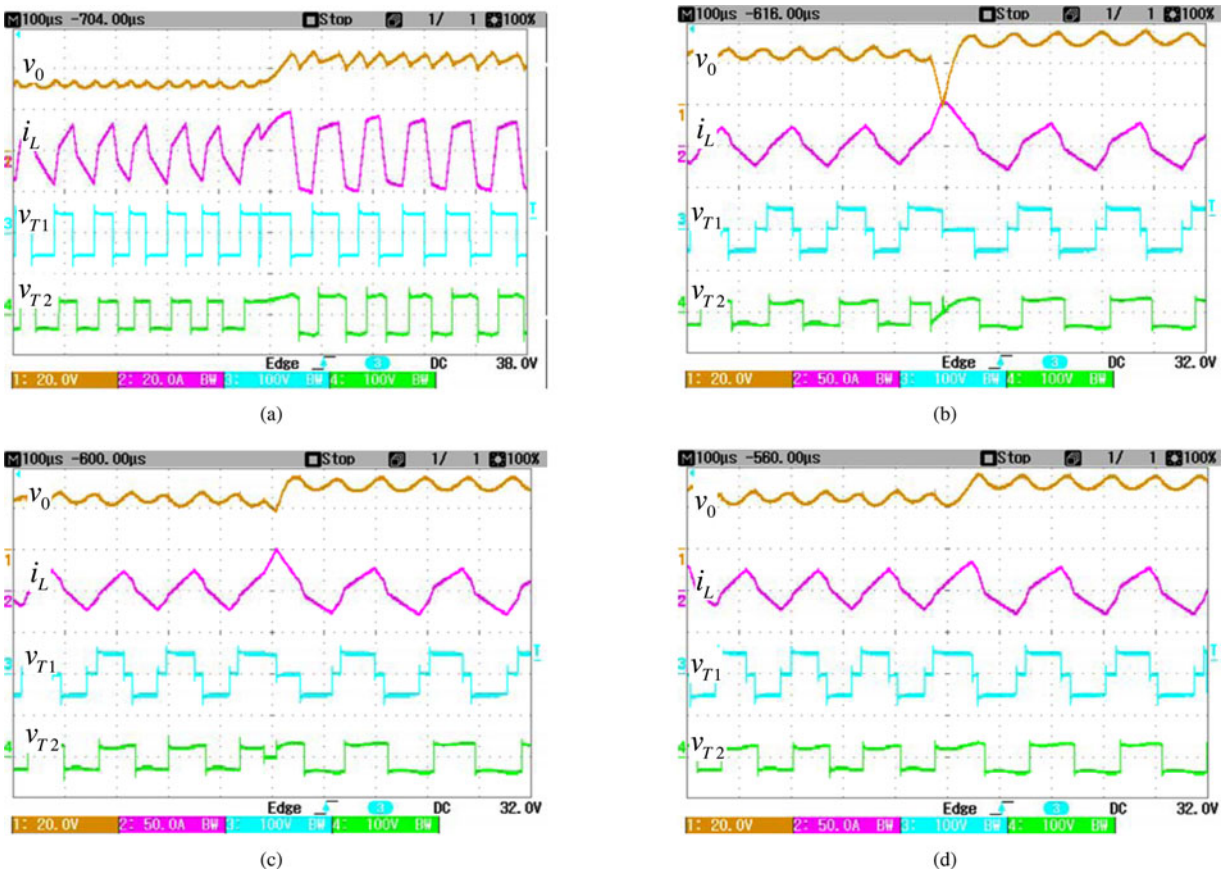

Fig. 15. Experimental evaluation of switching trajectories for a change of reference for buck mode: (a) strategy M1 switching sequence from 35 to 50 V. Strategy M2 from 25 to 35 V with trajectory (b) λ_1 (output voltage drop and current peak), (c) λ_2 for boost mode (current peak), and (d) λ_2 for buck mode (best trajectory selection with no voltage drop and moderate current). Output voltage (Ch1), inductor current (Ch2), primary voltage (Ch3), and secondary voltage (Ch4).

Fig. 15, it can be concluded that a proper selection of the switching sequences leads to behavior more conducive to reaching steady-state operation, thus validating the proposed strategy.

The experimental results presented in Fig. 16, obtained using the proposed switching sequence (M1, M2, and M3) and a variable frequency from 6 to 10 kHz, show the efficiency of the strategy compared to the conventional modulation strategy in boost mode with $V_{cc} = 50$ V and $V_o = 66$ V. The M1 strategy employs 6 kHz above 700 W, M2 strategy uses 8 kHz between 500 and 700 W and 10 kHz between 200 and 500 W, and M3 strategy is used from 50 to 200 W (burst mode). It can be concluded that efficiency gains are achieved for the whole operating range, from light to heavy loads, as a result of employing the proposes switching sequences.

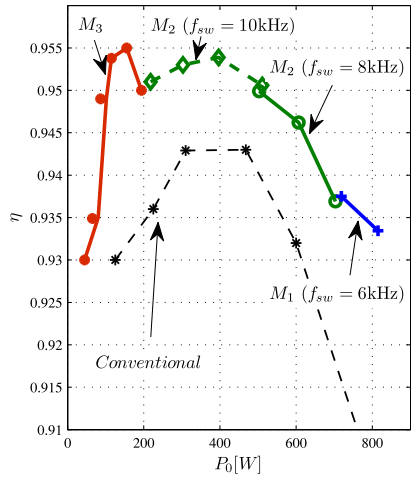

Fig. 16. Experimental efficiency gains, versus output power, employing M1, M2, and M3 switching sequences.

Burst mode (M3) is a discontinuous sequence strategy by definition. When the output power increases, the burst interval increases and the dormant interval decreases. Therefore, the overall losses from using the power switches and transformer are higher, resulting in lower efficiency. Fig. 15 is the experimental confirmation of the theoretical losses model presented in Fig. 5. It can be seen that the burst interval is small compared to the dormant interval.

V. Conclusion

This paper presented high-efficiency switching sequences based on the natural state-plane trajectories to reduce power losses in DAB converters. The analysis provided insight into the mechanisms to produce soft-switching transitions for light, medium, and heavy loading conditions while minimizing the RMS current levels to mitigate conduction losses. The theory and experimental validations revealed that careful selection of the switching sequence and frequency allows operation at improved efficiency levels. Burst mode was introduced to transfers power on-and-off for a few cycles under light loading condition, thus reducing unnecessary operation of the converter. As a result, three operating regions were selected namely, heavy (M1), medium (M2), and light (M3). Region M1 provided a minimal sequence with four soft-switching trajectories and moderately lower frequency; M2 employed a six trajectory strategy with moderately higher frequency and soft transitions; and M3 enabled an advantageous burst mode for efficient light loading operation. The experimental results obtained with a 1000-W prototype confirmed the operation of M1, M2, and M3 with their associated efficiency gains.

References

[1] P. Loh, D. Li, Y. Chai, and F. Blaabjerg, "Hybrid ACDC microgrids with energy storages and progressive energy flow tuning," *IEEE Trans. Power Electron.*, vol. 28, no. 4, pp. 1533–2543, Apr. 2013.

[2] D. Dong, I. Cvetkovic, D. Boroyevich, W. Zhang, R. Wang, and P. Mattavelli, "Grid-interface bidirectional converter for residential DC distribution systems—Part 1: High-density two-stage topology," *IEEE Trans. Power Electron.*, vol. 28, no. 4, pp. 1655–1666, Apr. 2013.

[3] D. Dong, I. Cvetkovic, D. Boroyevich, W. Zhang, R. Wang, and P. Mattavelli, "Grid-interface bidirectional converter for residential DC distribution systems—Part 2: AC and DC interface design with passive components minimization," *IEEE Trans. Power Electron.*, vol. 28, no. 4, pp. 1667–1679, Apr. 2013.

[4] A. Kuperman, I. Aharon, S. Malki, and A. Kara, "Design of a semi-active battery-ultracapacitor hybrid energy source," *IEEE Trans. Power Electron.*, vol. 28, no. 2, pp. 806–815, Feb. 2013.

[5] D. Segaran, D. G. Holmes, and B. P. McGrath, "Enhanced load step response for a bidirectional dc-dc converter," *IEEE Trans. Power Electron.*, vol. 28, no. 1, pp. 371–379, Jan. 2013.

[6] R. W. De Doncker, D. M. Divan, and M. H. Kheraluwala, "A three-phase soft-switched high-power-density dc/dc converter for high-power applications," *IEEE Trans. Ind. Appl.*, vol. 27, no. 1, pp. 63–73, Jan./Feb. 1991.

[7] F. Krismer and J. W. Kolar, "Accurate power loss model derivation of a high–current dual active bridge converter for an automotive application," *IEEE Trans. Ind. Electron.*, vol. 57, no. 3, pp. 881–891, Mar. 2010.

[8] G. G. Oggier, M. Ordonez, J. M. Galvez, and F. Luchino, "Fast transient boundary control and steady-state operation of the dual active bridge converter using the natural switching surface," *IEEE Trans. Power Electron.*, vol. 29, no. 2, pp. 946–957, Feb. 2014.

[9] X. She, X. Yu, F. Wang, and A. Q. Huang, "Design and demonstration of a 3.6-kV120-V/10-kVA solid-state transformer for smart grid application," *IEEE Trans. Power Electron.*, vol. 29, no. 8, pp. 3982–3996, Aug. 2014.

[10] H. Fan and H. Li, "High-frequency transformer isolated bidirectional dc-dc converter modules with high efficiency over wide load range for 20 kVA solid–state transformer," *IEEE Trans. Power Electron.*, vol. 26, no. 12, pp. 3599–3608, Dec. 2011.

[11] H. Qin and J. W. Kimball, "Solid-state transformer architecture using ac-ac dual–active–bridge converter," *IEEE Trans. Ind. Electron.*, vol. 60, no. 9, pp. 3720–3730, Sep. 2013.

[12] C. Zhao, S. Lewdeni-Schmid, J. K. Steinke, M. Weiss, T. Chaudhuri, M. Pellerin, J. Duron, and P. Stefanutti, "Design, implementation and performance of a modular power electronic transformer (PET) for railway application," *Proc. Power Electron. Appl*, 2011, pp. 1–10.

[13] M. H. Kheraluwala, R. W. Gascoigne, D. M. Divan, and E. D. Baumann, "Performance characterization of a high-power dual active bridge dc-to-dc converter," *IEEE Trans. Ind. Appl.*, vol. 28, no. 6, pp. 1294–1301, Nov./Dec. 1992.

[14] H. Bai and C. Mi, "Eliminate reactive power and increase system efficiency of isolated bidirectional dual-active-bridge dc–dc converters using novel dual-phase-shift control," *IEEE Trans. Power Electron.*, vol. 23, no. 6, pp. 2905–2914, Jun. 2008.

[15] G. G. Oggier, G. O. García, and A. R. Oliva, "Modulation strategy to operate the dual active bridge dc–dc converter under soft-switching in the whole operating range," *IEEE Trans. Power Electron.*, vol. 26, no. 4, pp. 1228–1236, Apr. 2011.

[16] H. Zhou and A. M. Khambadkone, "Hybrid modulation for dual-active-bridge bidirectional converter with extended power range for ultracapacitor application," *IEEE Trans. Ind. Appl.*, vol. 45, no. 4, pp. 1434–1442, Apr. 2009.

[17] A. K. Jain and R. Ayyanar, "PWM control of dual active bridge: Comprehensive analysis and experimental verification," *IEEE Trans. Power Electron.*, vol. 26, no. 4, pp. 1215–1227, Apr. 2011.

[18] F. Krismer and J. W. Kolar, "Closed form solution for minimum conduction loss modulation of DAB converters," *IEEE Trans. Power Electron.*, vol. 27, no. 1, pp. 174–188, Jan. 2012.

[19] F. Krismer and J. W. Kolar, "Efficiency-optimized high-current dual active bridge converter for automotive applications," *IEEE Trans. Ind. Electron.*, vol. 59, no. 7, pp. 2745–2760, Jul. 2012.

[20] B. Zhao, S. Qiang, and L. Wenhua, "Power characterization of isolated bidirectional dual-active-bridge dc-dc converter with dual-phase-shift control," *IEEE Trans. Power Electron.*, vol. 27, no. 9, pp. 4172–4176, Sep. 2012.

[21] T. Hirose, M. Takasaki, and Y. Ishizuka, "A power efficiency improvement technique for a bidirectional dual active bridge dc-dc converter at light load," *IEEE Trans. Ind. Appl.*, vol. 50, no. 6, pp. 4047–4055, Nov./Dec. 2014.

[22] J. Hiltunen, V. Visnen, R. Juntunen, and P. Silventoinen, "Variable-frequency phase shift modulation of a dual active bridge converter," *IEEE Trans. Power Electron.*, 2015, in press.

[23] X.-F. He, Z. Zhang, Y.-Y. Cai, and Y.-F. Liu, "A variable switching frequency hybrid control for ZVS dual active bridge converters to achieve

high efficiency in wide load range," in *Proc. IEEE Appl. Power Electron. Conf. Expo.*, 2014, pp. 1095–1099.
[24] F. Canales, T. H. Li, and D. Aggeler, "Novel modulation method of a three-level isolated full-bridge LLC resonant DC-DC converter for wide-output voltage application," in *Proc. 15th Int. Power Electron. Motion Control Conf.*, 2012, pp. 1–7.
[25] C. Fiorentino, Z. Hu, and Y.-F. Liu, "Improving the light load efficiency and THD of PFC converters using a line cycle skipping method," in *Proc. IEEE Control Modeling Power Electron.*, 2013, pp. 1–7.
[26] C. Fiorentino, Z. Hu, and Y.-F. Liu, "A line cycle skipping method to improve the light load efficiency and THD of PFC converters," in *Proc. IEEE Appl. Power Electron. Conf. Expo.*, 2013, pp. 368–373.
[27] G. G. Oggier, G. O. García, and A. R. Oliva, "Switching control strategy to minimize dual active bridge converter losses," *IEEE Trans. Power Electron.*, vol. 24, no. 7, pp. 1826–1838, Jul. 2009.
[28] A. Holz and H. Teuchert, "Die schule des elektrotechnikers - VII: Theorie, Berechnung Und Konstruktion der Transformatoren," *Leibpiz: Verlag Moritz-Schäfer*, 1963.
[29] T. Hatakeyama and K. Onda, "Core loss estimation of various materials magnetized with the symmetrical/asymmetrical rectangular voltage," *IEEE Trans. Power Electron.*, vol. 29, no. 12, pp. 6628–6636, Dec. 2014.
[30] W. A. Roshen, "A practical, accurate and very general core loss model for nonsinusoidal waveforms," *IEEE Trans. Power Electron.*, vol. 22, no. 1, pp. 30–40, Jan. 2007.

Germán G. Oggier (M'10) was born in Cordoba, Argentina. He received the Electr. Eng. and the M.Sc. degree in electrical engineering from the Universidad Nacional de Rio Cuarto, Rio Cuarto, Argentina, in 2003 and 2006, respectively, and the Doctor degree in control systems from the Universidad Nacional del Sur, Buenos Aires, Argentina, in 2009.

He was a Postdoctoral Fellow with Simon Fraser University, Metro Vancouver, BC, Canada, from 2011 to 2012 and with the University of British Columbia, Vancouver, BC, Canada, in 2014. His postdoctoral research activities include the area of boundary control of power converters. He is currently a Lecturer in the Grupo de Electronica Aplicada, Universidad Nacional de Rio Cuarto. He is also a Researcher with the Consejo Nacional de Investigaciones Cientificas y Tecnicas, Buenos Aires, Argentina. His current research interests include power electronics, electric vehicles, and renewable energy conversion.

Martin Ordonez (S'02–M'09) was born in Neuquen, Argentina. He received the Ing. degree in electronics engineering from the National Technological University, Cordoba, Argentina, in 2003, and the M.Eng. and Ph.D. degrees in electrical engineering from the Memorial University of Newfoundland (MUN), St. Johns, NL, Canada, in 2006 and 2009, respectively.

He is currently the Canada Research Chair in power converters for renewable energy systems and Assistant Professor with the Department of Electrical and Computer Engineering, University of British Columbia, Vancouver, BC, Canada. He was an adjunct Professor with Simon Fraser University, Burnaby, BC, and MUN. His industrial experience in power conversion includes research and development at Xantrex Technology Inc./Elgar Electronics Corp. (now AMETEK Programmable Power in San Diego, California), Deep-Ing Electronica de Potencia (Rosario, Argentina), and TRV Dispositivos (Cordoba, Argentina). With the support of industrial funds and the Natural Sciences and Engineering Research Council, he has contributed to more than 60 publications and R&D reports.

Dr. Ordonez is an Associate Editor of the IEEE TRANSACTIONS ON POWER ELECTRONICS, serves on several IEEE committees, and reviews widely for IEEE/IET journals and international conferences. He was awarded the David Dunsiger Award for Excellence in the Faculty of Engineering and Applied Science (2009) and the Chancellors Graduate Award/Birks Graduate Medal (2006), and became a Fellow of the School of Graduate Studies, MUN.